YGLF motif in the Kaposi sarcoma herpes virus G-protein- coupled receptor adjusts NF-kB activation and paracrine actions

S Azzi, Ss Smith, J Dwyer, Hm Leclair, C Alexia, Jk Hebda, N Dupin, N Bidère, J Gavard

Oncogene (2013), 1–10

www.nature.com/onc

ORIGINAL ARTICLE

YGLF motif in the Kaposi sarcoma herpes virus G-protein-coupled receptor adjusts NF-κB activation and paracrine actions

S Azzi[1,2,3,8], SS Smith[1,2,3,8], J Dwyer[1,2,3], HM Leclair[1,2,3], C Alexia[4,5,6], JK Hebda[1,2,3], N Dupin[3,7], N Bidère[4,5,6] and J Gavard[1,2,3]

Kaposi sarcoma (KS) and primary effusion lymphoma (PEL) are two pathologies associated with KS herpes virus (KSHV/HHV-8) infection. KSHV genome contains several oncogenes, among which, the viral G-protein-coupled receptor (vGPCR open reading frame 74) has emerged as a major factor in KS pathogenicity. Indeed, vGPCR is a constitutively active receptor, whose expression is sufficient to drive cell transformation *in vitro* and tumour development in mice. However, neither the role of vGPCR in KSHV-infected B-lymphocytes nor the molecular basis for its constitutive activation is well understood. Here, we show that vGPCR expression contributes to nuclear factor-κB (NF-κB)-dependent cellular survival in both PEL cells and primary B cells from HIV-negative KS patients. We further identified within vGPCR an AP2 consensus binding motif, Y_{326}GLF, that directs its localization between the plasma membrane and clathrin-coated vesicles. The introduction of a mutation in this site (Y_{326}A) increased NF-κB activity and proinflammatory cytokines production. This correlated with exacerbated morphological rearrangement, migration and proliferation of non-infected monocytes. Collectively, our work raises the possibility that KSHV-infected B-lymphocytes use vGPCR to impact ultimately the immune response and communication within the tumour microenvironment in KSHV-associated pathologies.

Oncogene advance online publication, 2 December 2013; doi:10.1038/onc.2013.503

Keywords: KSHV; vGPCR; NF-κB; trafficking; B-lymphocytes; HIV malignancies

INTRODUCTION

Kaposi sarcoma (KS) composes a class of heterogeneous pseudo-endothelial inflammatory tumours. These potentially malignant, widespread lesions are typically found in the skin, oral cavity, lymph nodes and visceral organs. Five epidemiologic subtypes of KS have been described: classic from the Mediterranean, Middle Eastern and Eastern European areas; endemic in subequatorial Africa; iatrogenic in immunosuppressed transplant patients; epidemic in AIDS-suffering patients; and rare in HIV-negative men who have sex with men.[1–3] Despite a reduction in incidence due to highly active antiretroviral therapies, KS remains one of the most common AIDS-associated malignancies.[2] This disease is caused by the KS herpes virus (KSHV/human herpes virus 8, HHV-8), and still remains incurable.[4–6] Besides KS, KSHV is linked to two aggressive lymphoproliferative disorders that affect the B-lymphocyte population, primary effusion lymphomas (PEL) and multicentric Castleman disease.[3,7–9] Currently, the only treatment available for PEL is a combination of chemotherapy and antiretroviral therapy in HIV-positive patients, with a median survival of 6 months.[9]

KSHV-associated lymphomas, like most non-Hodgkin's lymphomas, have developed a profound addiction to nuclear factor-κB (NF-κB) transcription factors. Indeed, abrogation of constitutive NF-κB activity is toxic for PEL *in vitro* and in mouse xenograft models.[10–12] Furthermore, NF-κB activation has also been proposed to transform endothelial cells and to convey paracrine transformation in models of KS, both *in vitro* and *in vivo*.[13–16] Among the proteins encoded by the KSHV, the homologue of FADD-like interleukin (IL)-1β-converting enzyme (FLICE/caspase-8) inhibitory protein (vFLIP, also known as K13) is a pivotal mediator of aberrant NF-κB activation.[11,17] Indeed, vFLIP binds and activates the IκB kinase complex, which phosphorylates the NF-κB inhibitor IκBα to precipitate its proteasomal degradation, thereby allowing NF-κB nuclear translocation.[18,19] Although transgenic mouse models have clearly established that forced vFLIP expression increases lymphoma incidence through uncontrolled NF-κB activation, vFLIP remains insufficient to fully recapitulate PEL phenotypes and fails to initiate KS-like lesions in animal models.[20–24] Therefore, it is tempting to speculate that vFLIP cooperates with other KSHV open reading frames (ORFs) and the host in the course of both sarcomagenesis and lymphomagenesis.

The ORF74, which encodes for a viral G-protein-coupled receptor (vGPCR), has emerged as an appealing candidate for oncogenic abilities of KSHV. vGPCR, a homologue of the human chemokine receptor CXCR2, harbours multiple point mutations, which render it constitutively active.[25–27] vGPCR is believed to be a key driver of KS, as it exhibits tumour-initiating and -transforming potential.[20,28–30] Indeed, vGPCR elicits survival, proliferation and migration in many cell models and signals through various molecular cascades, including the NF-κB and phosphatidylinositol 3-kinase/mammalian target of rapamycin pathways.[13,16,30–33] Moreover, vGPCR-directed NF-κB activation results in the secretion of proinflammatory cytokines that might be involved in paracrine communication.[16,34,35] Interestingly, vGPCR has also been shown to contribute to immune escape,[36] suggesting that this viral oncogene occupies strategic positions in the development of KSHV-related malignancies.

Although vGPCR-mediated control of NF-κB activation in pseudo-endothelial tumours and KS is well documented, whether

[1]CNRS, UMR8104, Paris, France; [2]INSERM, U1016, Paris, France; [3]Universite Paris Descartes, Sorbonne Paris Cite, Paris, France; [4]INSERM, U1014, Hopital Paul Brousse, Villejuif, France; [5]Universite Paris-Sud P11, Orsay, France; [6]Equipe Labellisee Ligue contre le Cancer, Villejuif, France and [7]Service de dermatologie, Hopital Cochin-Tarnier, AP-HP, Paris, France. Correspondence: Dr J Gavard, Institut Cochin, CNRS, UMR8104, INSERM U1016, Universite Paris Descartes, 22 rue Mechain, Room 306, Paris 75014, France.
E-mail: julie.gavard@inserm.fr
[8]These authors equally contributed to this work.
Received 4 June 2013; revised 25 September 2013; accepted 18 October 2013

its signalling activity is involved in B-lymphocyte homeostasis is largely unknown. Here, we provide evidence that vGPCR weighs into the regulation of the constitutive NF-κB activation and cell survival of both circulating primary B-lymphocytes in a lymphoma-free context and PEL cells. We further identify an AP2 binding motif (Y_{326}GLF) within the C terminus domain of vGPCR, which ensures its ability to fine-tune NF-κB activation and paracrine actions.

RESULTS

vGPCR drives NF-κB activation in primary B cells from KS patients

Although vGPCR is sufficient to initiate KS when expressed in the endothelial compartment,[37] its role in KSHV-infected circulating cells remains poorly documented. We first asked whether vGPCR expression could be involved in the homeostasis of primary B cells from KS patients, in a lymphoma-free context. To this end, vGPCR expression was examined by flow cytometry in B-lymphocytes (CD19), T-lymphocytes (CD3), monocytes (CD11) and macrophages (CD14) from peripheral blood mononuclear cells (PBMCs) from HIV-negative KS patients (Table 1). vGPCR was detected, independently of KS stages and viremia, in CD19-, CD11- and CD14-positive cells, but was absent from CD3-positive cells. Therefore, these data discriminate KSHV-infected circulating cell populations (i.e. positive B cells, macrophages and monocytes versus negative T cells) (Supplementary Table S1, Figure 1a and Supplementary Figure S1). The KSHV products, vGPCR, LNA (late-associated nuclear antigen) and RTA (replication and transcription activator), were present both in the CD19-positive fraction within total PBMCs and in purified CD19-positive cells (Figure 1b). Of note, the level of expression of latent and lytic KSHV products, namely LNA, vGPCR and RTA, was not altered when the CD19-positive cell population was isolated and cultured for 3 days (Figure 1c).

vGPCR can activate the NF-κB transcription factor, which in turn is known to modulate lymphoproliferation in KSHV-infected cells.[12,16] We therefore explored if the same was true in KSHV-infected primary B cells. First, levels of IκBα phosphorylation were significantly higher in the KSHV-positive, CD19-positive cell population, indicative of increased NF-κB activity (Figures 1d and e). Next, to determine its impact on IκBα phosphorylation, vGPCR was silenced in total or purified CD19-positive PBMCs from KS patients. Reduction in vGPCR expression correlated with decreased levels of phosphorylated IκBα, albeit LNA expression levels were not modified (Figure 1f). In addition, vGPCR silencing drove cell death in purified CD19-positive PBMCs (Figure 1g). Collectively, our data suggest that vGPCR contributes, at least partially, to NF-κB activation and survival of primary B cells from KS patients, even in the absence of lymphoproliferative disorders.

vGPCR contributes to the survival of NF-κB-dependent KSHV-infected PEL

PEL are characterized by a profound addiction to aberrant activation of NF-κB transcription factors.[38] However, whether vGPCR participates in this process remains unclear. We first took advantage of PEL-derived human cell lines, namely BC1, BC3, BCBL1 and CRO/AP6, which exhibited high levels of both lytic and latent KSHV-encoded gene expression at the RNA levels, when compared with those of KSHV-negative NF-κB-independent Burkitt's BJAB lymphoma cells (Figure 2a). As expected, phorbol 12-myristate 13-acetate treatment further enhanced lytic gene expression in these cell lines (Figure 2b). Flow cytometry analysis revealed that vGPCR was significantly expressed in PEL lines (Supplementary Table S2 and Figure 2c). Notably, vGPCR was found coexpressed in either LNA- or RTA-positive cells, suggesting

Table 1. Clinical data of KS patients

KS patients	*Age (years)*	*Gender*	*HIV status*	*Type of KS*	*Krigel classification*	*CD4 count (cells per mm^3)*	*HHV-8 viremia (copies per ml)*
Patient 1	52	M	Negative	Endemic	IV	352	+ (2400)
Patient 2	67	M	Negative	Classic	II	379	+ (40)
Patient 3	81	M	Negative	Classic	II	485	Negative
Patient 4	63	M	Negative	Iatrogenic	IV	N/A	+ (300)
Patient 5	58	M	Negative	Endemic	III	578	Negative
Patient 6	N/A	M	Negative	Classic	I	N/A	ULD
Patient 7	77	M	Negative	Classic	II	621	+ (1200)
Patient 8	82	M	Negative	Classic	I	748	+ (1000)
Patient 9	57	M	Negative	Iatrogenic	IV	451	+ (NQ)
Patient 10	69	F	Negative	Endemic	Remission	1200	ULD

Abbreviations: KSHV/HHV-8, Kaposi sarcoma herpes virus; KS, Kaposi sarcoma; N/A, not available; NQ, not quantifiable; PBMC, peripheral blood mononuclear cell; ULD, under the limit of detection. Clinical information of HIV-negative, KSHV-positive patients from whom PBMCs were isolated.

Figure 1. vGPCR drives NF-κB activation in primary B cells from KS patients. (**a**) PBMCs from KS patients (KSHV-positive) and healthy donors (KSHV-negative) were isolated and the expression of vGPCR was evaluated in CD19-, CD11-, CD3- and CD14-positive cell fractions by flow cytometry. Representative histograms are shown. Dashed histograms correspond to the isotype-matched control and grey histograms show vGPCR staining. (**b**) LNA, vGPCR and RTA total expression was examined in CD19-positive cell fractions from KSHV-positive PBMCs or in purified CD19-positive cells. Dashed histograms correspond to the isotype-matched control and grey histograms show antibody staining. (**c**) Latent and lytic viral products expression was examined by reverse transcription–PCR (RT–PCR) and flow cytometry (10 000 events) in CD19-positive cells at day 0 and day 3 postpurification. (**d**) pIκBα expression was examined in CD19-positive cell fractions from KSHV-negative and -positive PBMCs. Dashed histograms correspond to the isotype-matched control and grey histograms show antibody (Ab) staining (1 000 000 events). (**e**) Mean fluorescence intensity (MFI, 1 000 000 events) for patient (KSHV-positive, $n = 7$) and control (KSHV-negative , $n = 3$) samples were analysed using the PRISM statistical software: vGPCR ($P = 0.0027$), LNA ($P = 0.0018$) and pIκBα ($P = 0.0017$). (**f**) PBMCs from KS patients were isolated and transfected with either non-silencing duplexes sequence (sic) or vGPCR siRNA (si no. 3). Representative samples are shown. CD19-positive cell fraction of total PBMCs was analysed 72 h post-transfection by flow cytometry (upper panel). Alternatively, CD19-positive cells were purified before transfection (lower panel). Dashed histograms correspond to the isotype-matched control (Ig), grey and black histograms show antibody staining. (**g**) Cell survival in the purified CD19-positive cell population was assessed by flow cytometry, with DIOC6 staining (10 000 events). The percentage of DIOC6 stained cells is indicated. Data were normalised to cells nucleofected with the control siRNA (sic). Each panel is representative of three independent experiments.

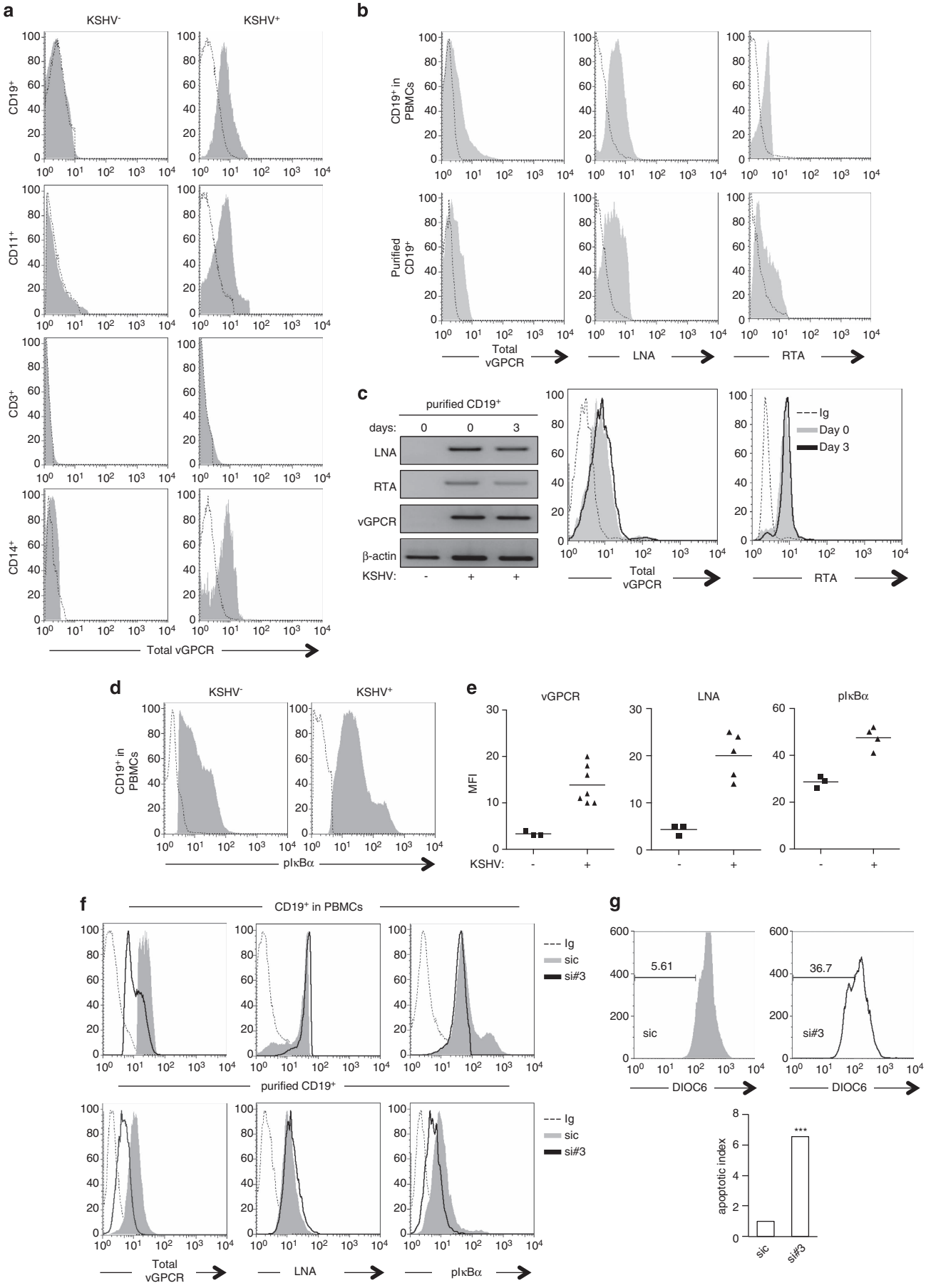

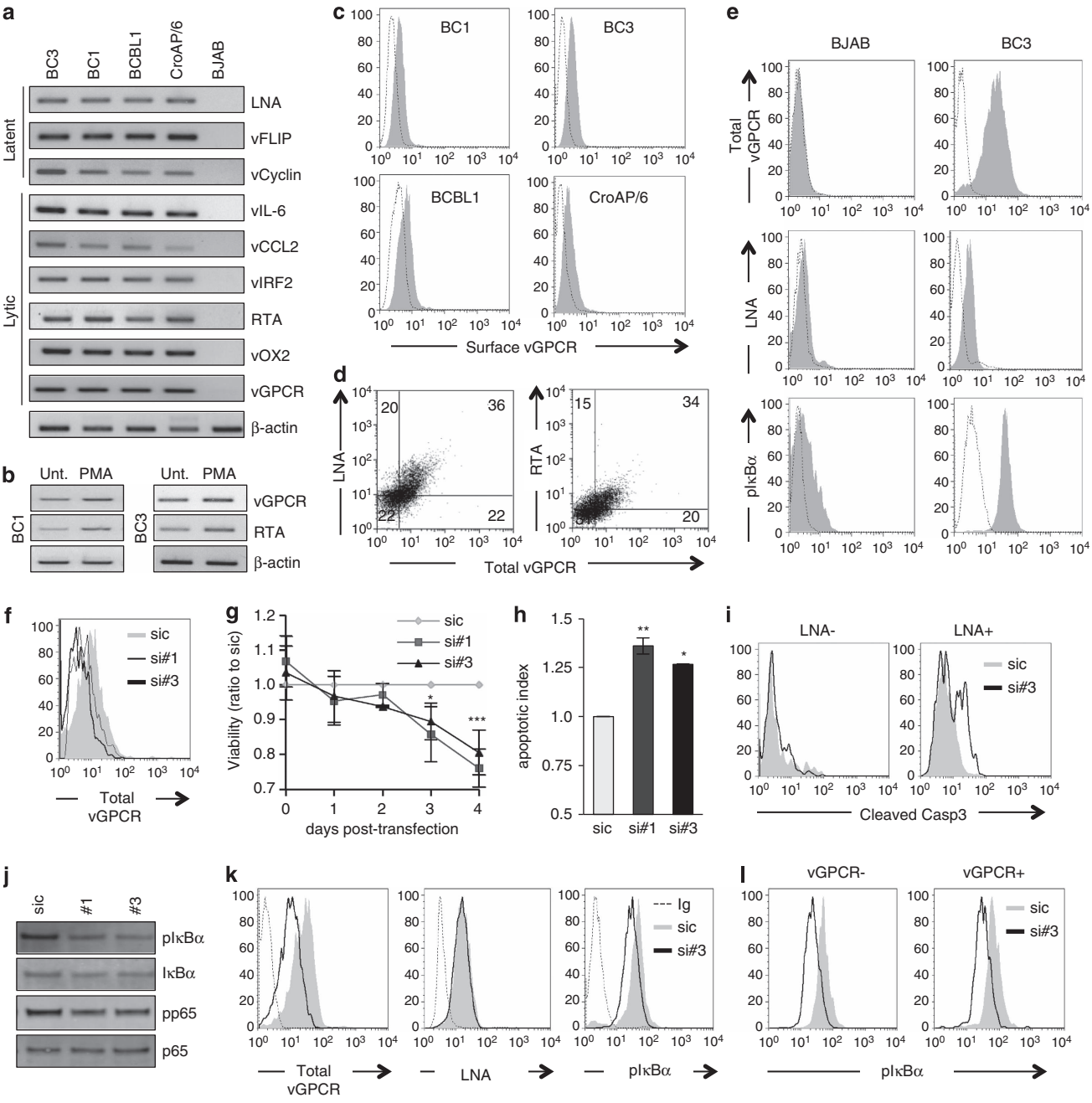

Figure 2. vGPCR contributes to the survival of NF-κB-dependent KSHV-infected BC3 PEL. (**a**) Latent and lytic gene expression levels were examined by reverse transcription–PCR (RT–PCR) in KSHV-infected PEL-derived cell lines (BC1, BC3, BCBL1 and CroAP/6). KSHV-negative BJAB cells were used as a negative control. (**b**) vGPCR and RTA expression levels were examined by RT–PCR in BC1 and BC3 cell lines treated or not with phorbol 12-myristate 13-acetate (10 ng/ml, 48 h). (**c**) BC1, BC3, BCBL1 and CroAP/6 were analysed by flow cytometry for surface vGPCR expression. Dashed histograms correspond to the isotype-matched control and grey histograms show vGPCR staining (10 000 events). (**d**) Latent and lytic viral products total expression was analysed in BC3 cells by flow cytometry. Dot plots show double staining of LNA/vGPCR and RTA/vGPCR (10 000 events). (**e**) vGPCR, LNA and pIκBα total expression were detected by flow cytometry in BC3 and BJAB cells. Dashed histograms correspond to the isotype-matched control (Ig) and grey histograms show antibody staining (10 000 events). (**f–l**) BC3 cells were transfected with vGPCR siRNA sequences (nos. 1 and 3) and processed 72 h later. Non-silencing duplexes sequence (sic) was used as a control. (**f**) siRNA efficiency was estimated by flow cytometry (10 000 events). (**g**) The effect of vGPCR silencing on proliferation of BC3 cells was analysed by the MTT assay. Values were normalised to sic-treated cells and expressed as a mean ± s.d. of three independent experiments. (**h**) Cell survival was determined by measuring the mitochondrial potential using DIOC6 probe in flow cytometry (10 000 events). Data were normalised to cells nucleofected with the control siRNA (sic). (**i**) The expression of the cleaved form of caspase-3 was determined in LNA-negative and LNA-positive BC3 cells using flow cytometry. Dashed histograms correspond to the isotype-matched control (Ig), grey and black histograms show antibody staining (10 000 events). (**j–l**) The levels of pIκBα, pp65, total IκBα and total p65 were determined by western blots and the expression of vGPCR, LNA and pIκBα by flow cytometry. Dashed histograms correspond to the isotype-matched control (Ig), grey and black histograms show antibody staining (10 000 events). Each panel is representative of three independent experiments.

that vGPCR can be detected in cells expressing latent and lytic markers (Figure 2d). This is reminiscent of the situation of infected lymphatic endothelial cells that exhibit a mixed latent/lytic programme.[39]

Paralleling our observations in B cells isolated from KS patients, PEL lines were characterized by phosphorylation of both IκBα and p65 (Figure 2e and Supplementary Figure S2). In addition, treatment with the IκB kinase inhibitor BMS-345541[40] selectively hampered PEL propagation (Supplementary Figure S2). To next determine its impact on PEL survival, vGPCR expression was silenced with two individual small interfering RNA (siRNA) sequences (Figure 2f). Interestingly, reducing vGPCR levels restrained PEL expansion and increased cell death, as illustrated by diminished mitochondrial activity in an MTT viability assay, reduced mitochondrial transmembrane potential as measured with a DIOC6 probe and the appearance of cleaved form of caspase-3 staining (Figures 2g–i). Interestingly, this caspase-3 processing was restrained to LNA-positive cells (Figure 2i). Furthermore, we found that knocking down vGPCR in PEL significantly reduced NF-κB reporter activity, as well as IκBα and p65 phosphorylation (Figures 2j–l and Supplementary Figures S3 and S4). In contrast, no obvious changes in LNA expression were observed in vGPCR-knockdown cells (Figure 2k). To define the relative contribution of vGPCR and vFLIP to the aberrant NF-κB activity in PEL, their expression levels were reduced with siRNA in BC3 cells and the phosphorylation of IκBα was evaluated by flow cytometry (Supplementary Figure S4). In both cases, the overall IκBα phosphorylation was decreased, albeit more pronounced when vFLIP was knocked down. Interestingly, this was further aggravated when both vFLIP and vGPCR were silenced. Lastly, enforced expression in HEK-293T cells of wild-type vGPCR, but not of R143A, a mutant unable to activate NF-κB, further enhanced vFLIP-induced NF-κB activation (Supplementary Figure S4). This argues for a basal activation of NF-κB through vGPCR, independently of vFLIP mode of action. Collectively, our results suggest that vGPCR and vFLIP operate independently to ensure the constitutive activation of NF-κB activation in KSHV-infected PEL cells and their continued survival.

vGPCR interacts within clathrin-coated vesicle components and YGLF motif governs vGPCR distribution

GPCR localization at the plasma membrane is tightly regulated by vesicular trafficking to prevent aberrant signalling.[41] For instance, CXCR2, the closest human homologue of vGPCR, is rapidly internalized upon chemokine stimulation (Figure 3a). However, vGPCR was found both at the cell surface and in an internal compartment (Figures 3a and b and Supplementary Figure S5). *In silico* analysis of vGPCR and CXCR2 sequences unveiled that vGPCR exclusively harbours a classical AP2 binding motif (Y_{326}GLF) in its C-terminal tail. We first explored the functionality of this motif in PEL cells. First, confocal analysis and immunoprecipitation experiments showed that vGPCR constitutively bound clathrin-coated vesicle (CCV) components, including AP2α, EPS15 and clathrin heavy chain (Figures 3b and c). Accordingly, a GST pull-down assay, conducted using either GST-vGPCR$_{321–342}$ or GST-CXCR2$_{321–360}$ C-tails as bait, demonstrated that vGPCR specifically interacted with CCV components (Figure 3d). We then investigated whether the loss of vesicular trafficking would result in the retention of vGPCR at the plasma membrane. To this end, both siRNA against AP2α and a dominant-negative EPS15 mutant (EPS15^{dn}) were used to block CCV formation and trafficking in endogenous (PEL cells; Figure 3e) and ectopic (vGPCR-transfected HeLa cells; Figures 3f and g) systems. As hypothesized, silencing AP2α led to an accumulation of vGPCR exposed at the plasma membrane (Figure 3e). Similarly, when overexpressed, vGPCR was found to accumulate in AP2α-positive vesicular structures. Likewise, while total vGPCR levels remained unchanged, its surface expression was increased in EPS15^{dn}-transfected cells (Figures 3f and g). Collectively, this suggests that a fraction of vGPCR is not available at the plasma membrane, but rather constitutively traffics within CCV.

Next, we generated an AP2 binding mutant (Y_{326}A) to determine whether the AP2 binding site coordinates vGPCR trafficking and localization. Although both wild-type (WT) and mutant (YA) constructs were expressed at similar levels in HeLa cells, only WT vGPCR co-immunoprecipitated with AP2α, demonstrating that the YA mutant is unable to bind to the AP2 complex (Figure 3h). Furthermore, flow cytometry analysis revealed that YA vGPCR surface staining was higher than WT vGPCR (Figure 3i). vGPCR movements were then tracked using an antibody uptake assay (Figures 3j and k). Although both were expressed at the plasma membrane, YA vGPCR distinguished from WT, as it barely accumulated in internal vesicles (Figures 3j and k). This suggests that basal vGPCR internalization is restrained in the YA mutant. Our results thus support the notion that the YGLF motif is required for vGPCR uptake into CCV, and therefore proper trafficking.

Abrogation of the YGLF motif alters NF-κB activation and vGPCR paracrine actions

We next tested whether the YGLF motif could also influence vGPCR-mediated NF-κB signalling activity. In HeLa cells, ectopic YA vGPCR triggered higher phosphorylation of IκBα when compared with WT vGPCR (Figure 4a). Moreover, the YA mutation markedly boosted the ability of vGPCR to activate NF-κB in a gene reporter assay (Figure 4b). To further characterize the functional effects of YA vGPCR expression, we next evaluated its paracrine actions on non-infected cells. Because NF-κB activation is strongly associated with enhanced transcription of key immune response-associated cytokines, we first checked the mRNA levels of IL-6, IL-8, IL-12α, IL-15 and tumor growth factor-β. YA vGPCR expression significantly increased the levels of IL-6, IL-8 and IL-15, whereas decreasing tumor growth factor-β (Figure 4c). To examine YA-mediated paracrine activity, conditioned media (CM) prepared from cells expressing either WT or YA vGPCR were tested on the KSHV-negative THP1 monocytes. Phosphorylation of IκBα was enhanced in THP1 cells treated with CM from YA-transfected cells when compared with either control or WT-derived CM (Figure 4d). In agreement, YA-CM significantly increased NF-κB promoter activity (Figure 4e). Moreover, when compared with the mock control, monocyte proliferation was enhanced by YA-CM (Figure 4f). YA-CM also significantly modified actin cytoskeleton organization and cell morphology, together with an increased ability to promote cell migration (Figures 4g and h). In comparison, WT-CM did not affect cell proliferation and had milder effects on monocyte morphology and migration (Figures 4f–h). Interestingly, endothelial permeability and T-cell migration were also enhanced using YA-CM (Supplementary Figure S6). Thus, the YA vGPCR-derived secretome is likely enriched in factors that promote a stronger proinflammatory phenotype than that of WT vGPCR. Our work provides evidence for the involvement of the vGPCR YGLF motif in the modulation of both NF-κB and paracrine actions, which might ultimately impact communication within the tumour microenvironment in KSHV-associated pathologies.

DISCUSSION

KSHV is the causative agent for both KS and two forms of high-grade non-Hodgkin's lymphomas, namely PEL and multicentric Castleman disease. Although vGPCR has emerged as a major viral actor in KS pathogenicity in endothelial cells, its role in infected B-lymphocytes still needs to be elucidated. In addition, how vGPCR evades negative feedback loops that normally curtail

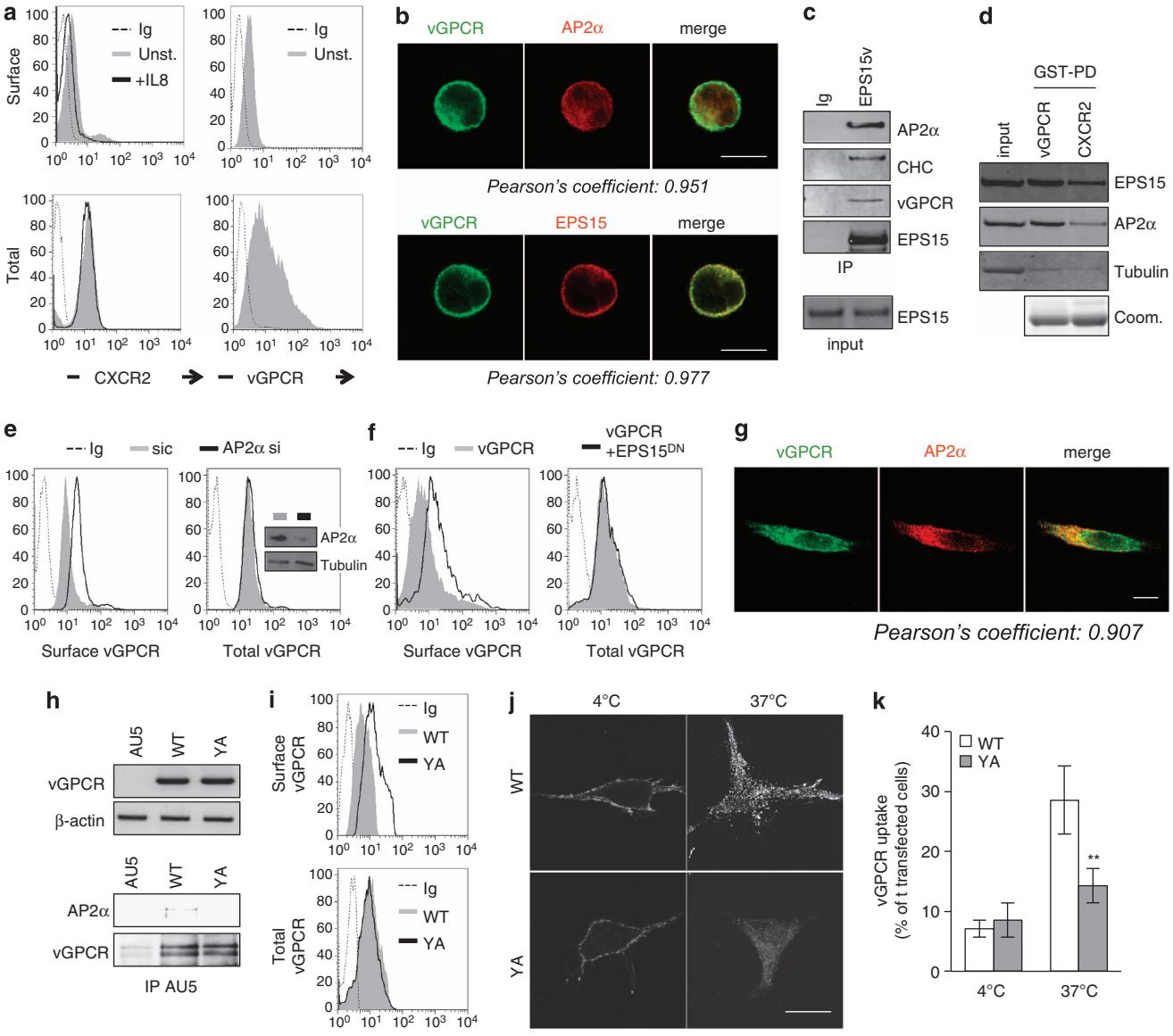

Figure 3. vGPCR interacts within CCV components. (**a**) BC3 were analysed by flow cytometry for surface and total CXCR2 and vGPCR expression before (unst.) and after IL-8 stimulation (+IL-8, 50 ng/ml, 30 min). Dashed histograms correspond to the isotype-matched control (Ig) and grey histograms show antibody (Ab) staining of 10 000 events. (**b**) BC3 cells were costained for vGPCR and either AP2α or EPS15 and further processed for confocal microscopy. Scale bars: 10 μm. (**c**) EPS15 immunoprecipitations were performed in BC3 cells. Interactions with CCV components were detected using antibodies against AP2α and clathrin heavy chain (CHC). In addition, vGPCR expression was analysed by western blots. Immunoglobulins (Ig) were used as a negative control. (**d**) HeLa protein lysates (input) were incubated with GST-tagged vGPCR and CXCR2 C-tails. EPS15 and AP2α expression was assessed by western blots. Tubulin was used a loading control. Levels of recombinant proteins were controlled by Coomassie Blue staining (Coom.). (**e**) BC3 cells were nucleofected with either non-silencing duplexes sequence (sic) or AP2α siRNA (AP2α si) for 72 h. siRNA efficiency was estimated by western blots against AP2α. Tubulin serves as a loading control. BC3 cells were stained with vGPCR and analysed by flow cytometry (10 000 events). Ig corresponds to the isotype-matched control. (**f**) HeLa cells were transfected with mock, a dominant-negative EPS15-GFP form ($EPS15^{dn}$), vGPCR or both $EPS15^{dn}$ and vGPCR constructs. Cells were analysed 24 h post-transfection using flow cytometry. Dashed histograms correspond to the isotype-matched control, grey and black histograms show monoclonal Ab staining of 10 000 events. (**g**) HeLa cells were transfected with vGPCR, costained for both vGPCR and AP2α, and then processed for confocal microscopy. Scale bars: 10 μm. (**h**) vGPCR expression levels were analysed by reverse transcription–PCR (RT–PCR) in HeLa cells transfected with AU5-tagged WT or YA vGPCR. An empty AU5 plasmid (AU5) was used as a control. AU5 immunoprecipitation (IP) fractions from HeLa cells transfected with AU5, AU5-tagged WT or YA vGPCR were assessed by western blots against vGPCR and AP2α. (**i**) HeLa cells were transfected with AU5, AU5-tagged WT or YA vGPCR and were analysed for total or surface vGPCR expression by flow cytometry. Dashed histograms correspond to the isotype-matched control (Ig), grey and black histograms show vGPCR staining of 10 000 events. (**j**) HeLa cells transfected with AU5-tagged WT or YA vGPCR were incubated with anti-vGPCR antibodies for 1 h at 4 °C (total) followed by 25 min incubation at 37 °C (uptake) before fixation. Scale bars: 10 μm. Graph represents the ratio between the number of cells with internal staining and the total number of transfected cells. $n > 200$, unpaired *t*-test: $^{**}P < 0.01$. Pearson's coefficient was measured using the Image J plugin. Each panel is representative of three independent experiments.

activated GPCRs is an open question. Here, we found that vGPCR expression contributes to constitutive NF-κB activation in B-lymphocytes, either from PEL cell lines or from lymphoma-free KS patients. We further identified a unique YGLF motif in the vGPCR C-terminus domain that adjusts its trafficking, NF-κB signalling activity and paracrine actions.

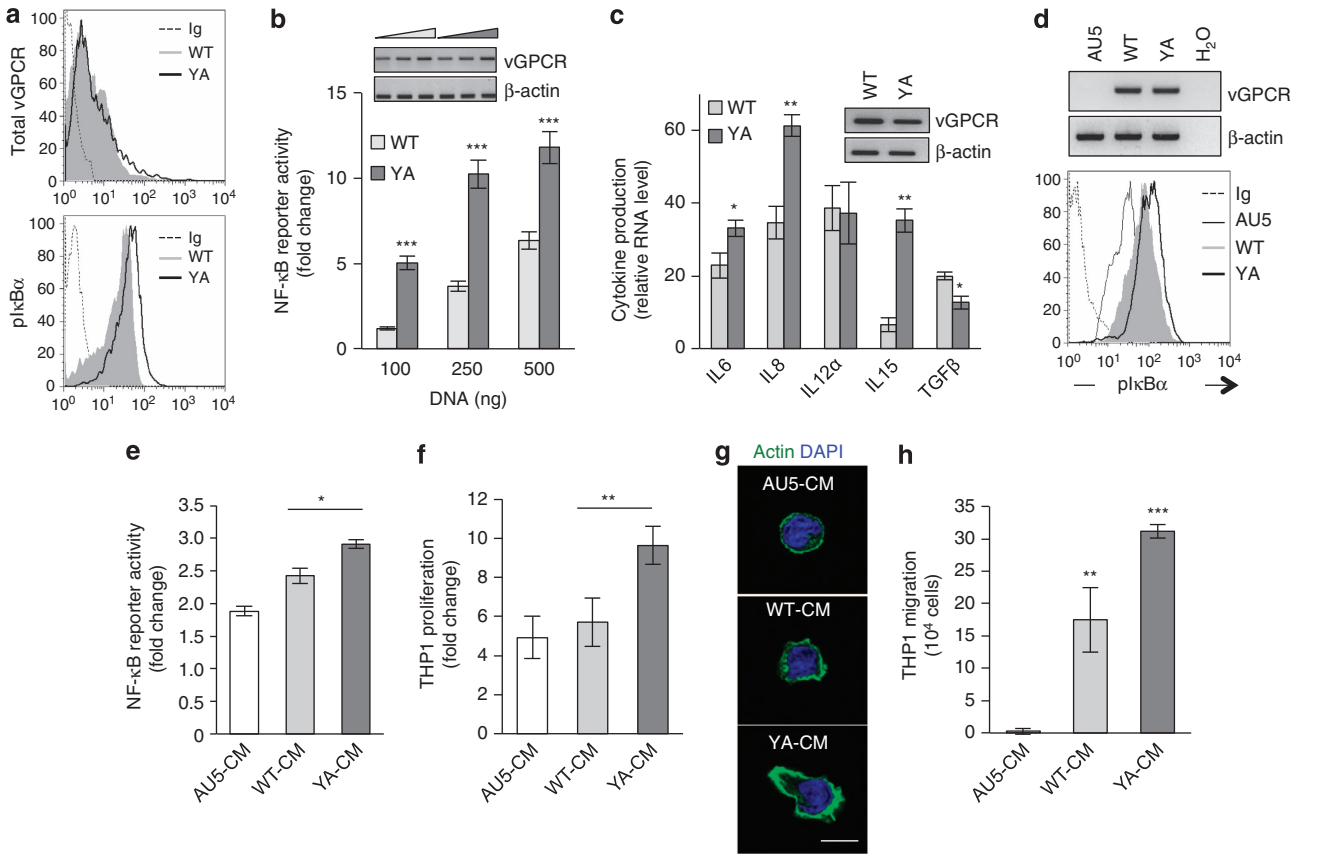

Figure 4. Abrogation of the YGLF motif alters NF-κB activation and vGPCR paracrine actions. (**a**) HeLa cells transfected with WT or YA vGPCR were analysed by flow cytometry for total vGPCR and pIκBα expression. Dashed histograms correspond to the isotype-matched control (Ig), grey and black histograms show antibody staining of 10 000 events. (**b**) NF-κB promoter activity was determined by a luciferase reporter assay in HEK-293T cells transfected with the indicated amounts of DNA of either WT or YA vGPCR constructs. Graph represents the mean ± s.d. from three experiments, unpaired *t*-test: ***$P<0.001$. (**c**) Cytokine profile as determined using reverse transcription–PCR (RT–PCR) on mRNA from HeLa cells transfected with either AU5-tagged WT or YA vGPCR constructs. Statistical analysis was conducted using the PRISM statistical software, using an unpaired *t*-test: **$P<0.01$, *$P<0.05$. (**d**) vGPCR expression was detected by reverse transcription–PCR (RT–PCR) in HeLa cells transfected with WT or YA vGPCR. β-Actin serves as a control. (**d–h**) THP1 monocytes were treated with CM collected from HeLa cells 24 h after transfection with AU5, WT vGPCR or YA vGPCR constructs. (**d**) FACS analysis of pIκBα expression. Dashed histograms correspond to the isotype-matched control, grey and black histograms show antibody staining of 10 000 events. (**e**) NF-κB promoter activity was determined by a luciferase reporter assay in THP1-Lucia monocytes. Graph represents the mean ± s.d. from three experiments normalized to untreated cells, unpaired *t*-test: *$P<0.05$. (**f**). THP1 cells were treated for 72 h and manually counted. Statistical analysis was conducted using the PRISM statistical software using a two-tailed unpaired *t*-test: **$P<0.01$. (**g**) THP1 cells treated for 72 h were stained with phalloidin and counterstained with DAPI. Actin morphology was examined by confocal microscopy. (**h**) THP1 migration was monitored in the presence of indicated CM for 3 h. Statistical analysis was conducted using two-tailed unpaired *t*-test: **$P<0.01$, ***$P<0.001$. Each panel is representative of three independent experiments.

vGPCR resembles the IL-8 receptor CXCR2, which operates as a potent chemoattractant for T-lymphocytes and neutrophils, and displays high angiogenic properties.[42] These pleiotropic functions ascribed to CXCR2 require strict control to avoid adverse effects in the organism. By contrast, vGPCR has evolved in a way that the viral receptor can be activated either upon ligand binding or in a ligand-independent manner, thereby exhibiting uninterrupted and constitutive activation.[25,26,31] When compared with the CXCR2 sequence and even to those of other human chemokine receptors, vGPCR exhibits multiple substitutions in key residues involved in conformational changes and G-protein coupling.[27,37] Here, we report the identification of a classical AP2 binding motif (Y_{326}GLF) within the intracellular C-terminus domain, unique to vGPCR. This site is indeed absent from human CXCR1, CXCR2 and CXCR4, and other viral GPCRs, namely BILF1 in EBV (Epstein–Barr virus), U12 and U51 in HHV-6A/B and HHV-7, and U27, U28, UL33 and UL78 in HCMV (human cytomegalovirus). Our results strongly support the idea that this motif is functional and drives vGPCR shuttling between the plasma membrane and CCV (Figure 3). Although we demonstrated that the YGLF motif is essential for vGPCR trafficking and downstream NF-κB activation, other key functions, including G-protein coupling, β-arrestin interaction, tyrosine sulfation and phosphorylation by GRKs remain to be investigated. Under physiological circumstances, GPCR missions are mainly terminated by internalization in CCV, where they can follow different fates: (i) fast targeting to lysosomes, (ii) rapid recycling back to the plasma membrane or (iii) retention in endosomes for a slow degradation or recycling process. The presence in the vGPCR C terminus domain of a binding motif for AP2, an integral CCV component, raises questions. One could imagine that because vGPCR is constitutively active, it has to evade physiological processes involved in desensitization. In this scenario, by constantly trafficking in CCV, vGPCR could escape stop signals normally operating on agonist-activated GPCRs. Accordingly, abrogation of the Y_{326}GLF motif stabilizes vGPCR at the plasma membrane. Unexpectedly, rather than normalization, the expression of the YA vGPCR mutant enhances the activation of NF-κB (Figure 4).

As many transforming abilities of vGPCR rely on NF-κB activity and paracrine signalling,[16] what could be the benefit for the virus to select a less active form? Cesarman and co-workers[35] have demonstrated that enforced expression of vGPCR augments not only NF-κB activity in PEL cells but also cell death, suggesting that exacerbated vGPCR signalling activity does not provide any selective advantage. In addition, the YA vGPCR-mediated elevated NF-κB activity was associated with an excessive inflammatory phenotype, as illustrated by cytokine production, monocyte and T-lymphocyte migration, monocyte spreading and proliferation, and endothelial permeability (Figure 4 and Supplementary Figure S6). It is worth noting that GPCRs exploited by other human viruses (as listed above) also mimic human receptors and foiled immune responses.[37] Therefore, strategies aimed at stabilizing vGPCR at the plasma membrane and blocking its low but constant cycling in CCV might be envisaged to raise an adapted immune response towards infected cells.

In this regard, B-lymphocytes could serve as a reservoir for KSHV, in both KS and lymphomas.[4,43,44] From a molecular standpoint, many signalling cascades downstream of vGPCR were found to be shared between B-lymphocytes and endothelial cells, including Gα-independent NF-κB activation.[13,31,45] However, the exact molecular route that turns on NF-κB in vGPCR-expressing cells is still under question. Importantly, we report here that primary B cells from KS patients exhibited high levels of NF-κB activation, even in a lymphoma-free context, whereas their survival is reduced upon vGPCR silencing (Figures 1 and 2). Selective expression of vGPCR in endothelial cells provokes inflammatory angiogenic KS-like lesions, where vGPCR-driven NF-κB activation may also have a role in tumour initiation and paracrine propagation.[13,16,20,28] Although it is established that PEL are highly dependent on NF-κB activation and that vFLIP might recapitulate this addiction,[11,17,22] our study now expands the possibility that cancerous and non-cancerous KSHV-infected B-lymphocytes co-opt vGPCR. Indeed, we show that both vFLIP and vGPCR are independently involved in NF-κB activation (Supplementary Figure S4). This argues in favour of a multi-parametric action of vGPCR in infected cells that is dependent on an intricate crosstalk between viral products, the host and the microenvironment.

In conclusion, KSHV-associated malignancies remain life-threatening cancers. The KSHV genome contains several pirated versions of cellular genes that are involved in cell cycle control, apoptosis blockade and paracrine/autocrine signalling, with vGPCR being one of its most prominent viral oncogenes. Further understanding of the molecular mechanisms of vGPCR in infected cells and in the tumour microenvironment will be beneficial to the development of new therapies for treating KSHV-governed diseases.

MATERIALS AND METHODS

Antibodies and reagents

Antibodies against CD19, CD11, CD14, CD3, CXCR2 and LAMP2, respective IgG isotype controls, phycoerythrin-conjugated rat anti-mouse IgG2a + b, AP2α, clathrin heavy chain and the Perm/Wash kit were obtained from BD (Le Pont de Claix, France). The following antibodies were used: IκBα, phospho-IκBα S32, phospho-IκBα S32/S36, phospho-NF-κB S536, GM130 and cleaved caspase-3 (Cell Signaling, Boston, MA, USA), EPS15, tubulin and NF-κB p65 (Santa Cruz, Heidelberg, Germany), AU5 (Covance, Rueil-Malmaison, France), kinectin (Millipore, St Quentin en Yvelines, France), LNA (Novocastra, Nanterre, France), vGPCR KSHV/HHV-8 ORF74 (R&D Systems, Lille, France) and RTA KSHV/HHV-8 ORF50 (antibodies online). AlexaFluor488 phalloidin, DIOC6, ProLong Gold Antifade Covance reagent with DAPI (4,6 diamidino-2-phenylindole) and secondary antibodies were obtained from Life Technologies (Saint Aubin, France). IL-8 was obtained from Peprotech (Neuilly-sur-Seine, France). IκB kinase inhibitor BMS-345541 (1.56–6.5 μM, 48 h) and phorbol 12-myristate 13-acetate (10 ng/ml, 48 h) were from Sigma (Lyon, France).

Ethics statement

HIV-negative, KSHV-positive (Table 1) and HIV-negative, KSHV-negative patients were followed by ND in the Dermatology Service (Cochin Hospital, Pavillon Tarnier, Paris, France). They all signed a written informed consent before sample collection, which occurred when providing a routine blood sample for diagnostic purposes. This study abides the rules of the Helsinki Protocol.

PBMCs isolation and purification

Fresh PBMCs were isolated using standard Ficoll-hypaque density centrifugation protocol (Ficoll-Paque; GE Healthcare, Velizy-Villacoublay, France). CD19-positive cells were purified by negative selection using magnetic cell sorting kit (Naive B cell isolation kit II; Miltenyi, Paris, France).

Cell culture, transfections and siRNA

BC3, BJAB, THP1, HeLa, Jurkat E6.1 and HEK-293T cells were purchased from ATCC (Molsheim, France). BC1, BCBL1 and CROAP/6 were obtained from DMSZ (Braunschweig, Germany) and THP1-Lucia NF-κB cells from Invivogen (Toulouse, France). Human umbilical vein endothelial cells were maintained as described previously.[33] DNA and siRNA were transfected using Turbofect (Fermentas, St Leon Rot, Germany) and Lipofectamine RNAiMax (Life Technologies), respectively. Alternatively, BC3 cells, total PBMCs and purified CD19-positive cells were nucleofected (Amaxa, Basel, Switzerland). CM were collected 24 h post-transfection and cleared by centrifugation and filtration. Non-silencing duplexes, predesigned MISSION siRNA sequences targeting human AP2α (EHU089461), duplexes designed against vGPCR (no. 1: 5′-UCUCAUAACACAUGGCCUG-3′ and no. 3: 5′-UCUGACAUGCAGUCGCCAG-3′) and vFlip (5′-AACGUGUUCAUACCUCAA CCC-3′) were purchased from Sigma.

DNA constructs

pCEFL-AU5 WT vGPCR construct,[33] pCEFL-AU5 R143A vGPCR construct,[46] pCEFL-HA-vFLIP[20] and pEGFP Δ95/295 deletion mutant Eps15 (EPS15^{dn}) construct[47] were described previously. The vGPCR Y_{326}A mutant was generated in pCEFL-AU5 backbone using site-directed mutagenesis (PFU Ultra; Life Technologies) and confirmed by sequencing (Beckman Coulter Genomics, Takeley, UK). vGPCR and human CXCR2 intracellular C-terminal tails (amino acids 321–342 and 321–360, respectively) were cloned in-frame into pGEX2-4 T plasmid between *Eco*RI and *Not*I.

Flow cytometry

For cell surface markers, cells were stained following an indirect (vGPCR) or direct (CD19, CD11, CD14, CD3 and CXCR2) immunofluorescence protocol. For intracellular staining (pS32-IκBα, RTA and LNA), cells were fixed using 1% paraformaldehyde and permeabilized by resuspension and vortexing in ice-cold methanol. Cells were incubated with primary antibodies, washed three times with cold phosphate-buffered saline and stained with the corresponding Alexa488- or phycoerythrin-conjugated IgG. For total vGPCR/CXCR2 staining, cells were first incubated with anti-vGPCR/CXCR2 antibodies, fixed in 1% paraformaldehyde, permeabilized with the Perm/Wash kit (BD) and processed for a second incubation with anti-vGPCR antibodies. For cell viability measurement, cells were incubated with DIOC6 (40 nM, 10 min, 37 °C) and immediately analysed by flow cytometry. Data were acquired on a FACScalibur (equipped with CellQuest software; BD) and processed with FlowJo (Ashland, OR, USA).

NF-κB luciferase reporter assay

NF-κB promoter activity was performed as described elsewhere[48] using the Dual-Luciferase Kit (Promega, Madison, WI, USA). Firefly fluorescence units were normalized to *Renilla* luciferase fluorescence units.

Western blots, GST pull-downs and immunoprecipitations

EPS15 and AU5 immunoprecipitations were performed as previously described.[33] For GST pull-downs, GST-fused peptides corresponding to $CXCR2_{321–360}$ and $vGPCR_{321–342}$ were affinity-purified on glutathione beads (Life Technologies), and incubated for 2 h with HeLa cell protein lysates, washed five times and analysed by western blot. Equal amounts of protein lysates, IP and GST fractions were separated onto 4–20% polyacrylamide Nupage gels (Life Technologies). Membranes were scanned using the Odyssey Infra-Red Imaging System (Li-Cor BioSciences, Lincoln, NE, USA).

Reverse transcription–polymerase chain reaction

RNA was extracted (Qiagen RNeasy Mini Kit) and equal amounts were reverse transcribed using the Superscript III RT kit (Life Technologies). Resulting cDNA was used to amplify vGPCR, LNA, vFLIP, vCyclin, vIL6, vCCL2, vIRF2, RTA, vOX2 and human IL-6, IL-8, IL-12α, IL-15, tumor growth factor-β and β-actin. mRNA was generated by polymerase chain reaction (PCR) in the presence of RedTaq Ready Mix (Sigma) using specific primer sets (Supplementary Table S3).

THP1 migration, proliferation and viability

Cell migration was determined with a 24-well Boyden chamber using a polyvinyl pyrrolidone-free polycarbonate filter with an 8 μm pore size (Nunc, Rochester, NY, USA) as described previously.[49] Cells that migrated into the CM-containing lower chamber were collected after 3 h and the cell number was manually counted in triplicate for each condition in four independent experiments. Proliferation was estimated by manual counts in THP1 (5×10^4) treated with CM for 72 h, and in triplicate for each condition in four independent experiments. Viability was evaluated with MTT (Sigma) and Uptiblue (Interchim, Montlucon, France), according to the manufacturer's instructions.

Immunofluorescence, Internalization assay and confocal microscopy

For HeLa cell imaging, staining was performed on cells grown on collagen-coated glass coverslips. For BC3 and THP1, cells were placed on poly-D-lysine-coated slides.[33] Internalization assay and immunofluorescence were conducted as described previously.[33] Cells were then mounted and analysed by confocal microscopy (TCS/SP5 Leica confocal microscope, Leica, Nanterre, France). Pearson's coefficient was measured using the Image J plugin (NIH, Besthesda, MD, USA).

Statistical analysis

All statistical analysis was performed using Graphpad Prism version 5.0c. Statistical analysis were carried out using one-way analysis of variance, two-way analysis of variance and an unpaired two-tailed *t*-test, as specified.

CONFLICT OF INTEREST

The authors declare no conflict of interest.

ACKNOWLEDGEMENTS

We thank the members of JG laboratory for comments on the manuscript. We are grateful to Dr A Benmerah (Institut Necker, Paris, France) for the EPS15 constructs and helpful discussion and to C Catherinet (INSA, Rennes, France) for technical support. This research was funded by: ANR JCJC, Fondation ARC, Fondation pour la Recherche Medicale, INCA_6508, Ligue nationale contre le cancer comite de Paris and a Marie Curie International Reintegration Grant within The Seventh Framework Program. SA, SSS and JD are supported by postdoctoral fellowships from Fondation ARC, Canceropole Ile-de-France and ANRS, respectively. JKH is supported by a doctoral fellowship from Universite Paris Descartes.

AUTHOR CONTRIBUTIONS

SA performed experiments, analysed data and drafted the manuscript; SSS performed experiments, analysed data and drafted the manuscript; JD performed experiments, analysed data and drafted the manuscript; HML performed experiments; CA performed experiments and analysed data; JKH performed experiments; ND collected clinical samples; NB analysed data and drafted the manuscript; JG designed research, performed experiments, analysed data and wrote the manuscript.

REFERENCES

1 Lanternier F, Lebbe C, Schartz N, Farhi D, Marcelin AG, Kerob D *et al.* Kaposi's sarcoma in HIV-negative men having sex with men. *AIDS* 2008; **22**: 1163–1168.
2 Lodi S, Guiguet M, Costagliola D, Fisher M, de Luca A, Porter K. Kaposi sarcoma incidence and survival among HIV-infected homosexual men after HIV seroconversion. *J Natl Cancer Inst* 2010; **102**: 784–792.
3 Mesri EA, Cesarman E, Boshoff C. Kaposi's sarcoma and its associated herpesvirus. *Nat Rev Cancer* 2010; **10**: 707–719.
4 Chang Y, Cesarman E, Pessin MS, Lee F, Culpepper J, Knowles DM *et al.* Identification of herpesvirus-like DNA sequences in AIDS-associated Kaposi's sarcoma. *Science* 1994; **266**: 1865–1869.
5 Boshoff C, Whitby D, Hatziioannou T, Fisher C, van der Walt J, Hatzakis A *et al.* Kaposi's-sarcoma-associated herpesvirus in HIV-negative Kaposi's sarcoma. *Lancet* 1995; **345**: 1043–1044.
6 Whitby D, Howard MR, Tenant-Flowers M, Brink NS, Copas A, Boshoff C *et al.* Detection of Kaposi sarcoma associated herpesvirus in peripheral blood of HIV-infected individuals and progression to Kaposi's sarcoma. *Lancet* 1995; **346**: 799–802.
7 Cesarman E, Nador RG, Aozasa K, Delsol G, Said JW, Knowles DM. Kaposi's sarcoma-associated herpesvirus in non-AIDS related lymphomas occurring in body cavities. *Am J Pathol* 1996; **149**: 53–57.
8 Mesri EA, Cesarman E, Arvanitakis L, Rafii S, Moore MA, Posnett DN *et al.* Human herpesvirus-8/Kaposi's sarcoma-associated herpesvirus is a new transmissible virus that infects B cells. *J Exp Med* 1996; **183**: 2385–2390.
9 Chen YB, Rahemtullah A, Hochberg E. Primary effusion lymphoma. *Oncologist* 2007; **12**: 569–576.
10 An J, Sun Y, Fisher M, Rettig MB. Antitumor effects of bortezomib (PS-341) on primary effusion lymphomas. *Leukemia* 2004; **18**: 1699–1704.
11 Matta H, Chaudhary PM. Activation of alternative NF-kappa B pathway by human herpes virus 8-encoded Fas-associated death domain-like IL-1 beta-converting enzyme inhibitory protein (vFLIP). *Proc Natl Acad Sci USA* 2004; **101**: 9399–9404.
12 Keller SA, Hernandez-Hopkins D, Vider J, Ponomarev V, Hyjek E, Schattner EJ *et al.* NF-kappaB is essential for the progression of KSHV- and EBV-infected lymphomas *in vivo*. *Blood* 2006; **107**: 3295–3302.
13 Montaner S, Sodhi A, Servitja JM, Ramsdell AK, Barac A, Sawai ET *et al.* The small GTPase Rac1 links the Kaposi sarcoma-associated herpesvirus vGPCR to cytokine secretion and paracrine neoplasia. *Blood* 2004; **104**: 2903–2911.
14 Grossmann C, Podgrabinska S, Skobe M, Ganem D. Activation of NF-kappaB by the latent vFLIP gene of Kaposi's sarcoma-associated herpesvirus is required for the spindle shape of virus-infected endothelial cells and contributes to their proinflammatory phenotype. *J Virol* 2006; **80**: 7179–7185.
15 Caselli E, Fiorentini S, Amici C, Di Luca D, Caruso A, Santoro MG. Human herpesvirus 8 acute infection of endothelial cells induces monocyte chemoattractant protein 1-dependent capillary-like structure formation: role of the IKK/NF-kappaB pathway. *Blood* 2007; **109**: 2718–2726.
16 Martin D, Galisteo R, Ji Y, Montaner S, Gutkind JS. An NF-kappaB gene expression signature contributes to Kaposi's sarcoma virus vGPCR-induced direct and paracrine neoplasia. *Oncogene* 2008; **27**: 1844–1852.
17 Guasparri I, Keller SA, Cesarman E. KSHV vFLIP is essential for the survival of infected lymphoma cells. *J Exp Med* 2004; **199**: 993–1003.
18 Liu L, Eby MT, Rathore N, Sinha SK, Kumar A, Chaudhary PM. The human herpes virus 8-encoded viral FLICE inhibitory protein physically associates with and persistently activates the Ikappa B kinase complex. *J Biol Chem* 2002; **277**: 13745–13751.
19 Field N, Low W, Daniels M, Howell S, Daviet L, Boshoff C *et al.* KSHV vFLIP binds to IKK-gamma to activate IKK. *J Cell Sci* 2003; **116**(Part 18): 3721–3728.
20 Montaner S, Sodhi A, Molinolo A, Bugge TH, Sawai ET, He Y *et al.* Endothelial infection with KSHV genes in vivo reveals that vGPCR initiates Kaposi's sarcomagenesis and can promote the tumorigenic potential of viral latent genes. *Cancer Cell* 2003; **3**: 23–36.
21 Chugh P, Matta H, Schamus S, Zachariah S, Kumar A, Richardson JA *et al.* Constitutive NF-kappaB activation, normal Fas-induced apoptosis, and increased incidence of lymphoma in human herpes virus 8 K13 transgenic mice. *Proc Natl Acad Sci USA* 2005; **102**: 12885–12890.
22 Ballon G, Chen K, Perez R, Tam W, Cesarman E. Kaposi sarcoma herpesvirus (KSHV) vFLIP oncoprotein induces B cell transdifferentiation and tumorigenesis in mice. *J Clin Invest* 2011; **121**: 1141–1153.
23 Boshoff C. Unraveling virus-induced lymphomagenesis. *J Clin Invest* 2011; **121**: 838–841.
24 Sin SH, Dittmer DP. Viral latency locus augments B cell response in vivo to induce chronic marginal zone enlargement, plasma cell hyperplasia and lymphoma. *Blood* 2013; **121**: 2952–2963.
25 Arvanitakis L, Geras-Raaka E, Varma A, Gershengorn MC, Cesarman E. Human herpesvirus KSHV encodes a constitutively active G-protein-coupled receptor linked to cell proliferation. *Nature* 1997; **385**: 347–350.
26 Bais C, Santomasso B, Coso O, Arvanitakis L, Raaka EG, Gutkind JS *et al.* G-protein-coupled receptor of Kaposi's sarcoma-associated herpesvirus is a viral oncogene and angiogenesis activator. *Nature* 1998; **391**: 86–89.
27 Rosenkilde MM, Kledal TN, Holst PJ, Schwartz TW. Selective elimination of high constitutive activity or chemokine binding in the human herpesvirus 8 encoded seven transmembrane oncogene ORF74. *J Biol Chem* 2000; **275**: 26309–26315.

28 Yang TY, Chen SC, Leach MW, Manfra D, Homey B, Wiekowski M *et al.* Transgenic expression of the chemokine receptor encoded by human herpesvirus 8 induces an angioproliferative disease resembling Kaposi's sarcoma. *J Exp Med* 2000; **191**: 445–454.
29 Bais C, Van Geelen A, Eroles P, Mutlu A, Chiozzini C, Dias S *et al.* Kaposi's sarcoma associated herpesvirus G protein-coupled receptor immortalizes human endothelial cells by activation of the VEGF receptor-2/ KDR. *Cancer Cell* 2003; **3**: 131–143.
30 Martin D, Galisteo R, Molinolo AA, Wetzker R, Hirsch E, Gutkind JS. PI3Kgamma mediates Kaposi's sarcoma-associated herpesvirus vGPCR-induced sarcomagenesis. *Cancer Cell* 2011; **19**: 805–813.
31 Couty JP, Geras-Raaka E, Weksler BB, Gershengorn MC. Kaposi's sarcoma-associated herpesvirus G protein-coupled receptor signals through multiple pathways in endothelial cells. *J Biol Chem* 2001; **276**: 33805–33811.
32 Smit MJ, Verzijl D, Casarosa P, Navis M, Timmerman H, Leurs R. Kaposi's sarcoma-associated herpesvirus-encoded G protein-coupled receptor ORF74 constitutively activates p44/p42 MAPK and Akt via G(i) and phospholipase C-dependent signaling pathways. *J Virol* 2002; **76**: 1744–1752.
33 Dwyer J, Le Guelte A, Galan Moya EM, Sumbal M, Carlotti A, Douguet L *et al.* Remodeling of VE-cadherin junctions by the human herpes virus 8G-protein coupled receptor. *Oncogene* 2011; **30**: 190–200.
34 Schwarz M, Murphy PM. Kaposi's sarcoma-associated herpesvirus G protein-coupled receptor constitutively activates NF-kappa B and induces proinflammatory cytokine and chemokine production via a C-terminal signaling determinant. *J Immunol* 2001; **167**: 505–513.
35 Cannon M, Philpott NJ, Cesarman E. The Kaposi's sarcoma-associated herpesvirus G protein-coupled receptor has broad signaling effects in primary effusion lymphoma cells. *J Virol* 2003; **77**: 57–67.
36 Lagos D, Vart RJ, Gratrix F, Westrop SJ, Emuss V, Wong PP *et al.* Toll-like receptor 4 mediates innate immunity to Kaposi sarcoma herpesvirus. *Cell Host Microbe* 2008; **4**: 470–483.
37 Montaner S, Kufareva I, Abagyan R, Gutkind JS. Molecular mechanisms deployed by virally encoded G protein-coupled receptors in human diseases. *Annu Rev Pharmacol Toxicol* 2013; **53**: 331–354.
38 de Oliveira DE, Ballon G, Cesarman E. NF-kappaB signaling modulation by EBV and KSHV. *Trends Microbiol* 2010; **18**: 248–257.
39 Chang HH, Ganem D. A unique herpesviral transcriptional program in KSHV-infected lymphatic endothelial cells leads to mTORC1 activation and rapamycin sensitivity. *Cell Host Microbe* 2013; **13**: 429–440.
40 Liu F, Xia Y, Parker AS, Verma IM. IKK biology. *Immunol Rev.* 2012; **246**: 239–253.
41 Marchese A, Chen C, Kim YM, Benovic JL. The ins and outs of G protein-coupled receptor trafficking. *Trends Biochem Sci* 2003; **28**: 369–376.
42 Waugh DJJ, Wilson C. The interleukin-8 pathway in cancer. *Clin Cancer Res* 2008; **14**: 6735–6741.
43 Hassman LM, Ellison TJ, Kedes DH. KSHV infects a subset of human tonsillar B cells, driving proliferation and plasmablast differentiation. *J Clin Invest* 2011; **121**: 752–768.
44 Myoung J, Ganem D. Active lytic infection of human primary tonsillar B cells by KSHV and its noncytolytic control by activated CD4 + T cells. *J Clin Invest* 2011; **121**: 1130–1140.
45 Cannon ML, Cesarman E. The KSHV G protein-coupled receptor signals via multiple pathways to induce transcription factor activation in primary effusion lymphoma cells. *Oncogene* 2004; **23**: 514–523.
46 Sodhi A, Montaner S, Patel V, Gomez-Roman JJ, Li Y, Sausville EA *et al.* Akt plays a central role in sarcomagenesis induced by Kaposi's sarcoma herpesvirus-encoded G protein-coupled receptor. *Proc Natl Acad Sci USA* 2004; **101**: 4821–4826.
47 Benmerah A, Bayrou M, Cerf-Bensussan N, Dautry-Varsat A. Inhibition of clathrin-coated pit assembly by an Eps15 mutant. *J Cell Sci* 1999; **112**(Part 9): 1303–1311.
48 Dwyer J, Hebda JK, Le Guelte A, Galan-Moya EM, Smith SS, Azzi S *et al.* Glioblastoma cell-secreted interleukin-8 induces brain endothelial cell permeability via CXCR2. *PLoS One* 2012; **7**: e45562.
49 Tan W, Martin D, Gutkind JS. The Galpha13-Rho signaling axis is required for SDF-1-induced migration through CXCR4. *J Biol Chem* 2006; **281**: 39542–39549.

Supplementary Information accompanies this paper on the Oncogene website (http://www.nature.com/onc)